IEEE Access
Multidisciplinary ⋮ Rapid Review ⋮ Open Access Journal

Received October 24, 2021, accepted October 30, 2021, date of publication November 2, 2021, date of current version November 10, 2021.

Digital Object Identifier 10.1109/ACCESS.2021.3125138

Trans-Domain Amphibious Unmanned Platform Based on Coaxial Counter-Propellers: Design and Experimental Validation

YONG GAO[1], HAO ZHANG[1,2], (Senior Member, IEEE), HUA YANG[1], SHIZHE TAN[1], T. AARON GULLIVER[2], (Senior Member, IEEE), AND TINGTING LU[1]

[1]Department of Electronic Engineering, Ocean University of China, Qingdao 266100, China
[2]Department of Electrical and Computer Engineering, University of Victoria, Victoria, BC V8W 2Y2, Canada

Corresponding author: Shizhe Tan (tanshizhe@ouc.edu.cn)

This work was supported in part by the Marine S and T Fund of Shandong Province for the Pilot National Laboratory for Marine Science and Technology, Qingdao, under Grant 2018SDKJ0210; in part by the National Natural Science Foundation of China under Grant 61701462 and Grant 41527901; in part by the Equipment for the Pre-research Field Fund Project under Grant 61404160502; in part by the Scientific Research Startup Foundation of Taishan University under Grant Y-01-2020016; and in part by the Fundamental Research Funds for the Central Universities under Grant 201713018.

ABSTRACT The rapid evolution of the Unmanned Aerial Vehicle (UAV) industry has significantly increased interest in UAV design with trans-domain capabilities. It is still a major challenge to achieve miniaturization and enhance the maneuverability and underwater reliability of trans-domain UAVs. In this paper, a novel bullet shape Trans-Domain Amphibious Vehicle (TDAV) is proposed which achieves free trans-domain motion and has the advantages of small size, high maneuverability and high reliability for both rotary-wing UAV and Autonomous Underwater Vehicle (AUV) operation. Compared with traditional amphibious machines, the TDAV design is streamlined and thus inherits the advantages of both the Bamboo Dragonfly and underwater AUVs. The proposed TDAV has a coaxial counter-propeller-tilting platform which satisfies the power and small diameter fuselage requirements, and the blades fold to reduce underwater drag and facilitate transportation. Further, a stable and efficient trans-domain attitude adjustment system is presented which effectively realizes trans-domain attitude switching. Based on the characteristics of the symmetric TDAV body, a rudder blade allocation algorithm is proposed to realize free movement in water. Finally, an improved particle swarm optimization algorithm is used to obtain suitable hierarchical fractional-order PID parameters. Both simulation and outdoor tests were performed and the results demonstrate that the proposed TDAV achieves outstanding performance in terms of lift altitude, trans-domain attitude switching time, and free trans-domain movement in both water and air.

INDEX TERMS Coaxial counter-propeller, trans-domain motion, amphibious vehicle, unmanned aerial vehicle, control strategies.

I. INTRODUCTION

Trans-domain aircraft have been the subject of research since the 1920s [1]. Conventional Unmanned Aerial Vehicles (UAVs) are highly maneuverable, non-contact, and can operate for long periods of time. Hence they are employed in a wide range of fields such as disaster relief, aerial video, agricultural production [2]–[4] and other civilian applications, as well as reconnaissance, targeting [5] and other military applications. Autonomous Underwater Vehicles (AUVs) have been instrumental in exploring the oceans [6] including bottom topographic surveying and investigating submarine hydrothermal sulfides. Recent advances in UAV technology and the increasing demands and number of applications have made trans-domain UAV with aerial cruise and covert underwater capabilities an important area of research.

In 2007, the Seagull series of surface drones was tested successfully [7]. Hydroplane taxiing was employed for take-off and landing. In [8], [9], an amphibious concept aircraft

The associate editor coordinating the review of this manuscript and approving it for publication was Jing Yan.

This work is licensed under a Creative Commons Attribution 4.0 License. For more information, see https://creativecommons.org/licenses/by/4.0/

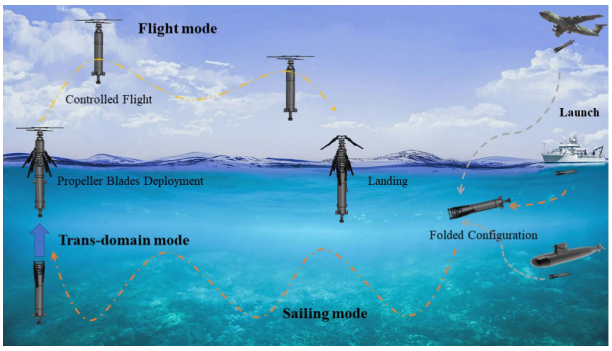

FIGURE 1. Illustration of the TDAV motion modes.

called Flying Fish with water glide landing capability was proposed. A prototype Flying Fish amphibious robot was presented in 2011 which also adopts glide takeoff and landing [10]. Sliding leap takeoff and landing is an effective way to provide water impact resistance for structures. However, this has problems such as time consumption and long takeoff and landing distance requirements which limit the applications.

In 2005, DARPA [11] commissioned the Cormorant UAV which employs splashdown to achieve trans-domain movement. In 2015, an amphibious trans-domain UAV was developed that mimics a skipjack to enable vertical takeoff and splashdown [12]. Test flights were conducted to validate the design. Splashdown water entry has advantages in terms of entry time and landing distance. However, the difference in density between air and water is about 800, so the significant impact force generated by the sudden change requires significant structural strength and impact resistance.

Recently, rotorcraft drones have been employed in underwater environments. Several prototypes have been developed such as Aquacopter [13], QuadH2o [14], Mariner [15], and HUAUV [16], [17]. These amphibious drones take off vertically from the water using the thrust of four rotor blades and can land smoothly on the water surface. However, they have poor underwater maneuverability and inconvenient storage which limits their applications.

In [18], a submarine deployable helicopter named Waterspout was proposed. A folding blade structure was adopted for stowage during transport and release is from the missile silo of the submarine. It is buoyant so it can float on the water and takes off vertically from the water surface using coaxial counter-propellers. However, this design has not been validated experimentally and the lack of active movement on the water makes Waterspout susceptible to currents that may prevent takeoff.

The emergence of UAVs with specialized shapes has motivated research on the design of the corresponding controllers. In [19], a robust neural network-based adaptive controller was proposed. This controller can effectively suppress external perturbations while following the desired trajectory. In [20]–[22], an algorithm based on sliding mode control was proposed to control a coaxial dual-rotor aircraft. A Gun-Launched Micro Air Vehicle (GLMAV) was designed in [23]–[25] based on a detailed aerodynamic analysis and the corresponding controllers were developed in [26]–[30]. In [31], [32], a ballistically-launched collapsible multi-rotor vehicle was designed and successfully tested outdoors.

In this paper, a novel Trans-Domain Amphibious Vehicle (TDAV) is proposed to mitigate the problems with previous approaches. It is designed to be impervious to water so drone operation in an aquatic environment does not require a capsule for protection. Both water takeoff and landing are vertical. This saves time and distance compared to taxiing and avoids the effects of water impact on the fuselage compared to splashdown. Different from rotorcraft UAVs, the TDAV flight system utilizes a coaxial counter-propeller-tilting platform structure with folding blades. This reduces the flow resistance in water and facilitates stowage and transportation. Compared to GLMAV, the proposed TDAV has a bullet shape with a more slender body. This expands the possible underwater applications and facilitates barrel boost realization. Further, it overcomes the technical challenges of Waterspout and has the maneuverability to effectively move in water. Thus, the proposed TDAV provides improved unmanned system capabilities in naval operations as shown in Fig. 1, and will lead to future advances in TDAV systems.

The contributions of this paper are as follows.

- A novel trans-domain amphibious UAV is proposed which has a bullet shape. A coaxial counter-propeller-tilting platform structure is adopted to provide sufficient power and also fit within a small diameter airframe which is waterproof. A hierarchical fractional-order PID control algorithm using improved particle swarm optimization is developed to determine the flight control parameters.
- To provide TDAV trans-domain motion, an Energy-Attitude Multiplexing (EAM) system is designed. further, a new acceleration and deceleration control algorithm is proposed to improve switching between trans-domain modes.
- A novel rudder blade allocation algorithm is proposed as conventional cross-shaped and X-shaped allocation methods cannot provide suitable attitude movement when the TDAV is rolling on the water due to its symmetry.
- A TDAV prototype was developed and the performance of each component was verified. A lake test was conducted which verifies that the TDAV can travel freely in both air and water. All test results met the design specifications.

The rest of the paper is organized as follows. Section II introduces the system concept including TDAV movement. The challenges and solutions in the development of the system platform are discussed in Section III. The results of the outdoor experiments and discussion are presented in Section IV, and Section V provides some concluding remarks.

FIGURE 2. Version 2.0 of the TDAV platform.

II. SYSTEM CONCEPT

As previously mentioned, a Trans-domain Amphibious Vehicle (TDAV) is proposed with a bullet shape and the ability to travel freely through air and water. The TDAV motion modes are divided into three parts: flight, trans-domain, and sail, for the purposes of implementation. Version 2.0 of the platform is shown in Fig. 2 (a) sail mode, and (b) flight mode with the propeller fully deployed and (c) top view.

In flight mode, the TDAV can hover like a conventional multi-rotor aircraft. However, the flight module converts to a coaxial counter-propeller-tilting platform to improve climbing efficiency. Further, adjusting the rotational speed of both rotors and varying the inclination angle of the platform provides both rotational and translational movement. When the TDAV leaves the water, the rudder fins remain upright to increase the aerodynamic damping during yaw motion which reduces the spin effect caused by the coaxial counter-propeller structure.

Trans-domain is the key mode for movement between water and air and to ensure suitable amphibious functionality. Fig. 1 shows that when the TDAV navigates underwater, the EAM module dynamically adjusts the position of the center of gravity on the fuselage axis to balance force and torque so the head (propeller) remains upright at all times. The coaxial counter-propeller motor provides flight power so the folded propeller blades can overcome water resistance and allow the TDAV to achieve trans-medium out-of-water movement.

Sail mode is for motion in water and has six degrees of freedom, namely pitch, roll, yaw, and x, y and z directions as will be explained later. The folding wing structure ensures a streamlined fuselage which reduces the resistance in water. As with conventional underwater vehicles, the tail thruster and tail fin of the TDAV are the primary mechanisms for underwater movement. They adjust the attitude of the fuselage in water while the flight mechanism is in silent (standby) mode.

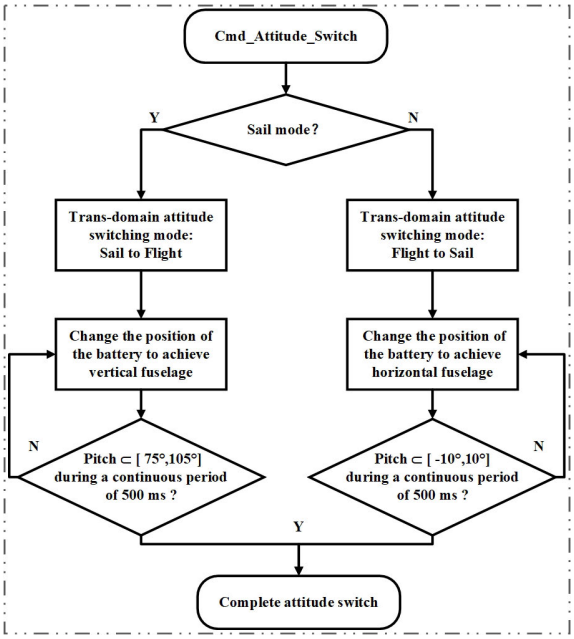

FIGURE 3. TDAV mode switching flowchart.

Switching between motion modes is critical for TDAV trans-domain motion and a flowchart for this is shown in Fig. 3. The steps for switching between the three modes are as follows.

1) If the initial state is sail mode, the stepper motor adjusts the center of gravity so that the body pitch is within = $\pm 30°$ in conjunction with the underwater power module for underwater attitude movement.
2) According to the navigation destination and trans-domain attitude switching mode, the stepper motor adjusts the position of the center of gravity of the fuselage so the pitch is 90°.
3) When the attitude sensor detects that the body pitch is $90° \pm 15°$ for 500 ms, the TDAV switches into flight mode. The coaxial counter-propeller motor starts to rotate and the folded blades open due to centrifugal force so the initial gravity and buoyancy equilibrium state is broken. When the motor reaches the required RPM, the TDAV moves out of the water due to the lift force and flight begins.
4) After the flight mission, the TDAV slowly descends into the water and the propellers close to the sides of the fuselage due to the mechanical tension springs.
5) When the depth sensor in the nose detects that the fuselage is below the water surface, the trans-domain attitude mode changes and the stepper motor adjusts the body pitch to 0°.
6) When the attitude sensor detects a body pitch of $\pm 10°$ for 500 ms, the TDAV switches to underwater sail mode.
7) Go to step 1.

The TDAV is designed to have three sections with waterproofing between them using O-ring seals. Fig. 4 shows the

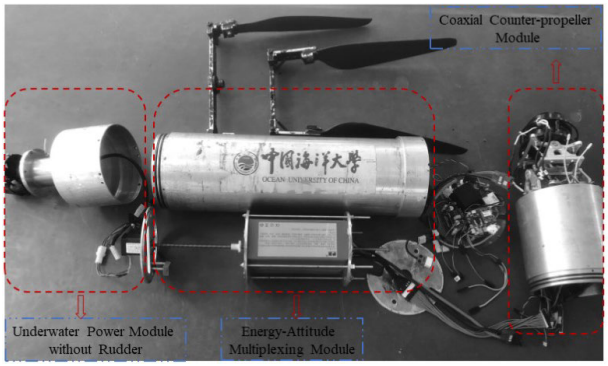

FIGURE 4. The TDAV components.

TABLE 1. The TDAV mass distribution.

Element	Number	Mass (kg)	Proportion (%)
Motor	2	1.20	18.0
Servomotor	2	0.14	2.1
Blade	4	0.50	15.0
Battery pack	1	3.80	28.5
Electronics module	1	0.20	1.5
Servo	4	0.04	1.2
Thruster	1	1.20	9.0
Machined component	1	3.30	24.7

TDAV components and an assembled CAD view is given in Fig. 5. Table 1 gives the mass of the TDAV elements determined using Solidworks modeling. This shows that the fuselage accounts for 24.7% of the mass while the battery accounts for 28.5%. It would be difficult to reduce the TDAV mass without affecting the trans-domain motion.

III. TDAV PLATFORM

The TDAV platform was the key part of the TDAV development process. Due to the unique structure of the TDAV, numerous implementation challenges had to be overcome. The three main challenges were: 1) the design of the flight power module for the bullet-shaped structure, 2) the design of the trans-domain attitude switching module for vertical takeoff and landing, and 3) the design of the underwater movement power module. The difficulties associated with these challenges as well as the solutions developed are presented in this section.

A. TDAV FLIGHT POWER CONFIGURATION

The design and development of the flight dynamics portion of the TDAV platform is presented in this section.

1) MECHANICAL ASPECTS

The TDAV platform is about twice as long as the GLMAV [27] in terms of the aspect ratio, so the TDAV fuselage is narrow. Thus, the traditional two-motor driven coaxial mechanism adopted in the GLMAV system cannot meet the flight design requirements. As a consequence, a new coaxial counter-propeller motor was developed for TDAV

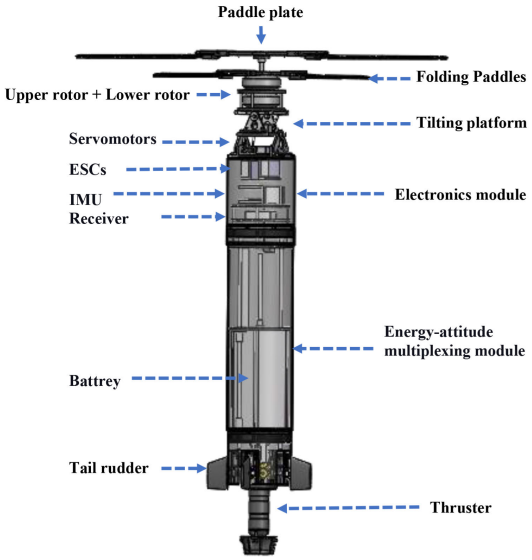

FIGURE 5. CAD view of the final version of the TDAV platform.

FIGURE 6. Parameters of a single rotor of a coaxial counter-propeller motor.

trans-domain motion. Different from traditional motors, it has an upper and lower coaxial structure so the diameter is less than 160 mm with a total lifting force of more than 40 kg, and is waterproof. The coaxial counter-propeller motor is shown in Fig. 6. The parameters for an individual motor are given in Table 2. This shows that when the throttle is 100%, the maximum pull is over 20 kg, the maximum current is over 100 A, and the maximum power is over 5000 W.

Compared with conventional rotorcraft, the coaxial counter-propeller motor is simpler and more compact. Further, it makes the TDAV weight more concentrated at the center of gravity which reduce the rotational inertia during trans-domain attitude switching. The coaxial counter-propeller structure means the upper and lower rotors rotate around the same axis in different directions. The torque required for yaw motion of the vehicle is generated by the total pitch difference between the rotors, eliminating the need for a tail rotor and providing higher hovering efficiency than conventional rotorcraft. To meet the requirements of both small diameter and waterproof, a new flight attitude adjustment structure was developed. This structure is similar to a gimbal as it vectorizes the direction of the head of the TDAV

TABLE 2. The coaxial counter-propeller motor parameters.

Throttle (%)	Pull-up (kg)	Pull-down (kg)	Current (A)	Power (W)
0	0	0	0	0
10	2.25	2.25	4.0	175.4
20	3.33	3.33	6.9	2140
30	5.55	5.55	14.0	2730
40	7.60	7.60	22.6	3208
50	9.82	9.82	33.0	3613
60	11.93	11.93	44.5	3958
70	14.10	14.10	58.3	4280
80	16.41	16.41	72.1	4570
90	18.57	18.57	90.0	4845
100	20.80	20.80	104.5	5080

by turning the servo to generate torque. For stability reasons, the maximum tilt angle is set to no more than 15°. The above structures are collectively called the coaxial counter-propeller-tilting platform.

A folding design was used for the rotor considering the amphibious TDAV characteristics and the coaxial counter-propeller motor. When the motor is stationary, the tension spring structure folds the blades close to the body to improve symmetry and facilitate navigation in water. In flight mode, the blades open smoothly due to the centrifugal force generated by the motor rotation. To avoid collisions between the upper and lower propellers during initial rotation and to ensure sufficient lift, a design with a shorter lower propeller disc and longer lower propeller clamps (as shown in the propeller structure in Fig. 4), was adopted after several tests and improvements.

Numerical simulations of TDAV in air and water environments were carried out with the help of the Fluent software package to find the appropriate parameters for the design to improve the motion performance (See Appendix A). The simulation results are an excellent basis for designing the TDAV body, but the long fuselage and low center of gravity makes it prone to swaying during flight. This must be corrected by the control algorithm.

2) FLIGHT CONTROL STRATEGY

The flight control algorithm is critical to stable TDAV flight in the air. However, unlike the traditional swashplate structure of the well-known coaxial twin-rotor aircraft [33]–[35], the TDAV adopts a tilting platform structure for air attitude adjustments. Thus, an effective TDAV flight control algorithm must be developed.

To design a suitable control strategy for the TDAV, a detailed dynamic model was constructed from the corresponding mechanical, fluid mechanics, and aeromechanics parameters. The relevant coordinate frames and main variables required for modeling are shown in Fig. 7. Table 3 gives the mathematical expressions for the model parameters.

The TDAV is an underdriven, nonlinear complex system with four degrees of freedom control inputs and six degrees of freedom outputs. The upper and lower rotors provide the thrust and the tilting angle of the tilting platform provides the

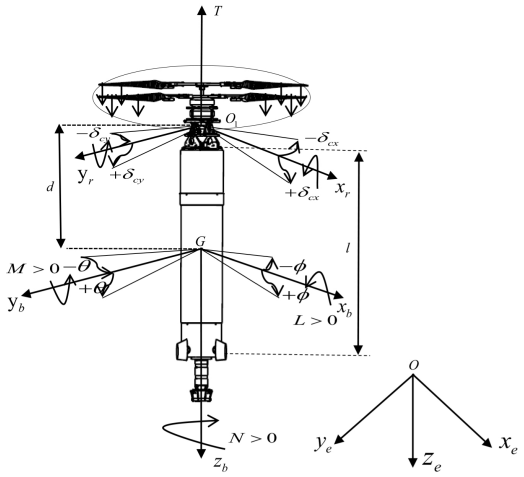

FIGURE 7. Related frames and parameters of TDAV.

TABLE 3. Definitions of symbols used in a dynamic model.

Parameter	Variable
Position in the inertial frame	$\zeta = [x, y, z]^T$
Velocity in the inertial frame	$v = [v_x, v_y, v_z]^T$
Acceleration in the inertial frame	$a = [a_x, a_y, a_z]^T$
Euler angle in the inertial frame	$\eta = [\phi, \theta, \psi]^T$
Angular velocity in the body frame	$\omega = [\omega_x, \omega_y, \omega_z]^T$
Motor thrust under the body frame	$T = [T_x, T_y, T_z]^T$
Motor torque under the body frame	$\Gamma = [M_x, M_y, M_z]^T$
Inertial matrix	$J = \text{diag}\,[J_{xx}, J_{yy}, J_{zz}]$
Transformation matrix	R_η
Platform tilt angle	δ_{cx}, δ_{cy}
Mass and mass reciprocal	m, Λ
Upper and lower motor speeds	Ω_1, Ω_2
Aerodynamic coefficients	$\gamma_1, \gamma_2, \alpha, \beta$
Distance between O_1 and G	d
Gravity acceleration	g

torque control. The changes in position, velocity, angle, and angular rate are represented by $\{O, x_e, y_e, z_e\}$ in the inertial coordinate frame and $\{G, x_b, y_b, z_b\}$ in the body coordinate frame.

To simplify the analysis and thus reduce the difficulty of controller design, some model approximations are used. The aerodynamic effects between the upper and lower propellers and the air resistance acting on the fuselage are neglected during hovering. However, this will be considered as an external perturbation in the simulation analysis. The equations for the forces and moments on the TDAV can then be expressed as

$$\begin{bmatrix} T_z \\ M_x \\ M_y \\ M_z \end{bmatrix} = \begin{bmatrix} \left(\alpha\Omega_1^2 + \beta\Omega_2^2\right)\cos\delta_{c_x}\cos\delta_{c_y} + mg\cos\theta\cos\phi \\ -d\alpha\Omega_1^2\sin\delta_{cy}\cos\delta_{c_x} - d\beta\Omega_2^2\sin\delta_{cy}\cos\delta_{c_x} \\ d\alpha\Omega_1^2\cos\delta_{c_x}\cos\delta_{c_y} + d\beta\Omega_2^2\cos\delta_{c_x}\cos\delta_{c_y} \\ \gamma_1\Omega_1^2 + \gamma_2\Omega_2^2 \end{bmatrix} \tag{1}$$

The TDAV control signals are $\Omega_1^2 = \frac{T_z - \beta\Omega_2^2}{\alpha}$, $\Omega_2^2 = \frac{\alpha M_z - \gamma_1 T_z}{\alpha\gamma_2 - \beta\gamma_1}$, $\delta_{cx} = -\frac{M_y}{d\alpha\Omega_1^2 + d\beta\Omega_2^2}$, and $\delta_{cy} = \frac{M_x}{d\alpha\Omega_1^2 + d\beta\Omega_2^2}$ which are represented by the control input T_z, $\Gamma\left(M_x, M_y, M_z\right)^T$.

Due to the complexity of the coaxial counter-propeller and tilting platform structures, and the problem of autonomous control in the presence of external disturbances, a hierarchical fractional-order PID (FOPID) control algorithm is employed. The inner loop of this algorithm provides FOPID control while the outer loop is conventional PID control. An improved Particle Swarm Optimization (PSO) algorithm is proposed to determine the FOPID control parameters. The flight control block diagram is shown in Fig. 8.

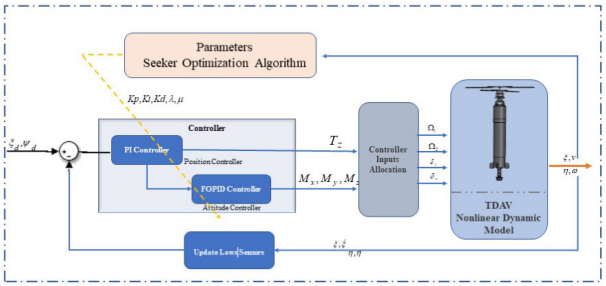

FIGURE 8. Closed-loop control block diagram of the TDAV flight control system.

The time and frequency domain expressions for the FOPID controller [36] are

$$u(t) = K_p e(t) + K_i \mathcal{D}^{-\lambda} e(t) + K_d \mathcal{D}^{\mu} e(t) \quad (2)$$

$$G(s) = K_p e(t) + K_i s^{-\lambda} + K_d s^{\mu} \quad (3)$$

where K_p is the proportional gain, K_i is the integral gain, K_d is the differential gain, and λ and μ are the orders of the integral and differential controllers, respectively, $\lambda, \mu \in (0, 1)$. Since FOPID have two more parameters than traditional PID controllers, they can provide better control robustness [37]. However, more parameters can make parameter tuning more difficult. Methods for optimizing the PID control parameters were proposed in [38], [39]. In this paper, a PSO algorithm is used to obtain the hierarchical FOPID parameters of the attitude control loop (See Appendix B).

Disturbance rejection is important for effective TDAV control. Fig. 9 presents the step response for the conventional PID (green dashed line), fractional-order PID (blue solid line) and proposed hierarchical fractional-order (red solid line) PID control algorithms. Fig. 9(a) shows that the response of the conventional algorithm is fast, but the overshoot is large (53%) and the time to steady-state is long. The proposed algorithm has a smaller overshoot (0.5%) and significantly faster time to steady-state. Fig. 9(b) shows that the proposed algorithm has excellent response to an external disturbances.

The PSO algorithm was executed 50 times and the best parameters were chosen as the final PID parameters. These parameters are used in the system model for motion simulation. Fig. 10 gives position and orientation of the aircraft during flight for the commanded position $\{x_d(t), y_d(t), z_d(t), \psi_d(t)\}$. This shows that the proposed hierarchical FOPID controller (red dashed lines) has a faster rise time, and a shorter time to steady-state than the conventional

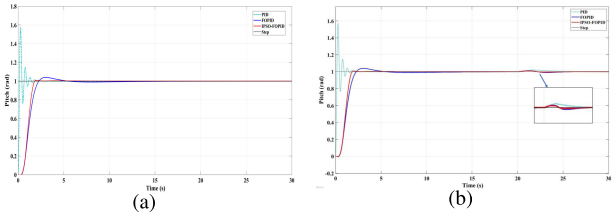

FIGURE 9. Pitch of the proposed hierarchical fractional-order, conventional PID, and fractional-order PID control algorithms: (a) step response, (b) disturbance response.

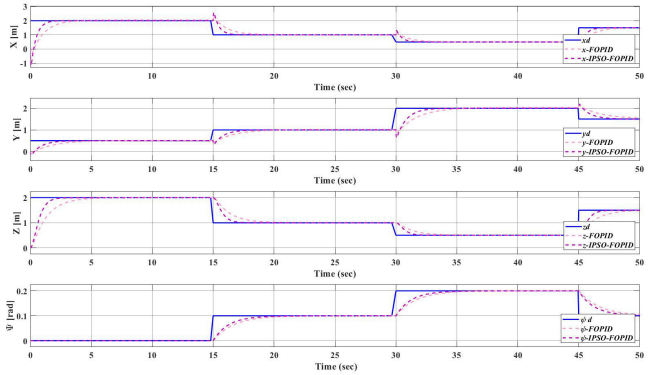

FIGURE 10. Position with the proposed hierarchical and conventional FOPID algorithms.

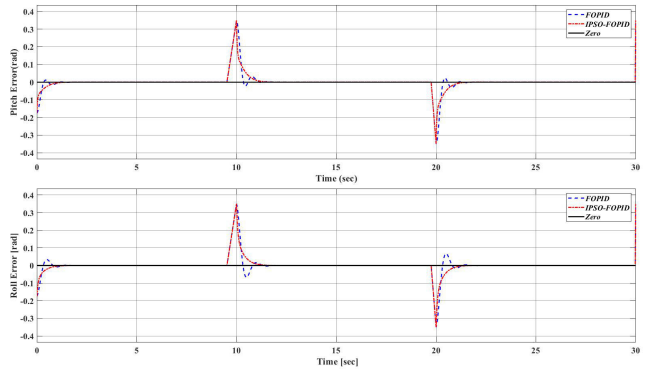

FIGURE 11. Trajectory error with the proposed hierarchical and conventional FOPID algorithms.

FOPID controller (green dashed lines). Fig. 11 presents the trajectory error, i.e. variations in (ϕ, θ), using the proposed hierarchical and conventional FOPID controllers to improve the effectiveness of the proposed control strategy. This effectiveness will be verified experimentally in the next section.

B. TDAV ATTITUDE SWITCHING CONFIGURATION

Effective attitude switching performance is important to successful TDAV trans-domain movement. Therefore, the configuration of the TDAV attitude switching mode is a key design challenge. An Energy-Attitude Multiplexing (EAM) system was designed for the TDAV to enable rapid vertical takeoff and landing during trans-domain motion.

1) MECHANICAL ASPECTS

Fig. 5 shows that the EAM module is located in the middle of the TDAV fuselage with the electronics compartment at

the top and the underwater power module at the bottom. The electronics module consists of a mainboard, inertial measurement unit (IMU), and processor module. The EAM is the TDAV energy source as well as a key component required for trans-domain mobility. The center of gravity is changed by a stepper motor moving the battery pack on the body axis to achieve attitude switching in trans-domain motion. The battery pack must meet the following conditions for trans-domain motion: 1) ability to drive the coaxial counter-propeller motor, 2) lifetime greater than 10 min, and 3) airframe symmetry in flight mode. The battery pack was customized to meet these specifications and the parameters are given in Table 4.

FIGURE 12. The custom battery.

TABLE 4. Custom battery parameters.

Parameter	Value
Name	TDAV-Bat-12S
Capacity	12000 mAh
Discharge rate	20 C
Nominal voltage	44.4 V
Fully charged voltage	50.4 V
Instantaneous discharge current	240 A
Continuous discharge current	180 A
Dimensions	186 × 103 × 75 mm

The power requirements of the coaxial counter-propeller motor and the underwater thruster are significant and they have different input voltages. This poses stability and safety challenges for the circuit design. To meet these challenges, multi-stage step-down voltage conversion with isolation is employed. The custom battery is shown in Fig. 12. It is hollow in the middle so the stepper motor can easily move the battery pack. However, precise control of the stepper motor is necessary for successful TDAV motion attitude adjustment. Further, the speed of this motor will determine the speed of motion attitude adjustment.

2) ATTITUDE SWITCHING CONTROL STRATEGY

The stepper motor must precisely control the battery pack. However, conventional speed control methods may lead to step loss or overshoot which will affect TDAV attitude regulation. Thus, an improved S-curve acceleration/deceleration control algorithm is proposed for this purpose. There are two main types of S-curve control algorithms, one that employs a specific S-curve [40]–[42], and another that employ separate S-curves for acceleration and deceleration. The S-curve stepper motor speed control function employed here is

$$f(x) = A + B\tanh(a \times x + C) \tag{4}$$

where $a = 1/2$ is the tilt parameter which adjusts the slope of the linear part of the curve, and scaling and translation is achieved by adjusting A, B, and C. Fig. 13 illustrates this function for different values of a with $A = 0$, $B = 1$, and $C = 0$. This shows that it has a symmetric S shape which is suitable for the stepper motor.

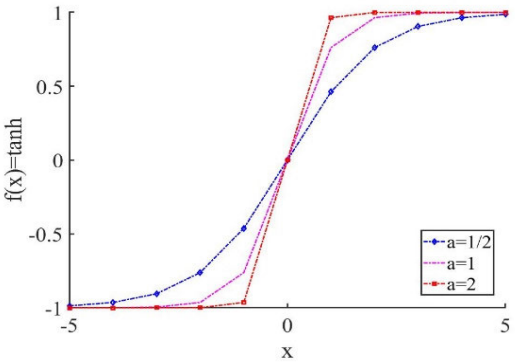

FIGURE 13. The stepper motor speed control function with different tilt parameters *a*.

The tanh function is complex to implement, which is a problem for real-time control systems. Thus, values of $f(x)$ were discretized and stored in a lookup table. The acceleration ratios in an array, and calculating the pulse frequency required for each step before the motor is controlled. It also achieves ''closed-loop'' control by combining with position sensors to further improve control accuracy.

A STM32F405RGT6 processor and DRV8825 stepper motor driver were used for speed regulation of a two-phase four-wire hybrid stepper motor. The stepping angle of this motor is 1.8°. For smooth motor operation, the master clock frequency of 84 Mhz was divided into four, is used as the clock frequency of the timer. Further, division by 16 is employed with the stepper motor driver so the angular displacement of a pulse is 0.1125°. Test results are presented in Section IV.

C. UNDERWATER POWER CONFIGURATION

Unlike Waterspout, the TDAV has the ability to move underwater. The underwater power module is composed of four tail rudder pieces and a thruster. The tail rudder employs dynamic sealing for waterproofing and operations based on attitude adjustment control commands are used to achieve underwater movement.

The TDAV is mechanically symmetrical which ensures that the center of gravity and center of flotation are on the same vertical axis. However, this symmetry makes the cross-shaped and X-shaped rudder blade distributions used in conventional AUVs unsuitable due to the effect of water resistance. Further, the TDAV is susceptible to cross-rolling, which makes these traditional rudder blade configurations inadequate for attitude movement in water. Therefore, an effective means of underwater motion must be designed. The solution is a new rudder blade allocation

algorithm that enables effective attitude movement in water with non-cross and non-X-shaped arrangements. Fig. 14 shows the conventional cross-shaped and X-shaped rudder blade arrangement [43]–[45] with the parameters given in Table 5. The X-shaped rudder is obtained by rotating the cross-shaped rudder 45° clockwise or counterclockwise.

TABLE 5. Rudder parameters.

Parameter	Variable
Rudder blade angle	δ_i
Hydrodynamic force on the rudder blade	R_i
Horizontal rudder angle	δ_s
Vertical rudder angle	δ_r
Differential rudder angle	δ_d
Fuselage cross-roll angle	β_m

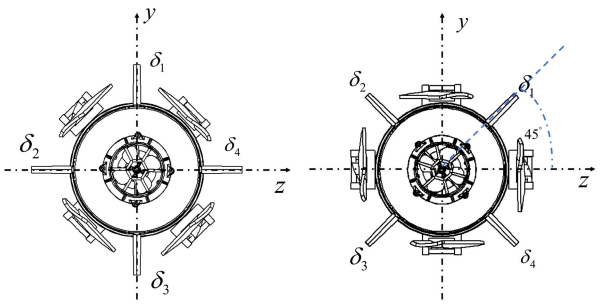

FIGURE 14. Cross-shaped rudder (a), and X-shaped rudder (b).

Cross-roll occurs due to the forces from water resistance as shown in Fig. 15. It is assumed that δ_1 is clockwise at an angle β_m which can be measured by the on-board sensors. The tail rudder generates a hydrodynamic force in the dynamic coordinate system G_{xyz}. Considering only the effect of the tail rudder on yaw and pitch, and ignoring the force in the x-direction, the hydrodynamic components in the G_{yz} plane are R_1, R_2, R_3 and R_4. Assuming a tail-to-head view from the TDAV, define δ_1 and δ_3 as positive on the right lower rudder and δ_2 and δ_4 as positive on the left lower rudder. Then, the forces Y and Z in the y and z directions are

$$\begin{aligned} Y &= -R_1 \cos\beta_n - R_2 \cos\beta_m - R_3 \cos\beta_n - R_4 \cos\beta_m \\ Z &= R_1 \sin\beta_n - R_2 \sin\beta_m + R_3 \sin\beta_n - R_4 \sin\beta_m \end{aligned} \quad (5)$$

where $R_i = R_i^0 \delta_i$ and R_i^0 is the hydrodynamic force on rudder δ_i for one degree. Assuming that the tail rudder blade areas are the same and ignoring the differences in the rudder flow fields, and defining $R_i^0 = k_x$, the above expression can be rewritten as

$$\begin{aligned} Y &= k_x\,(-\delta_1 \cos\beta_n - \delta_2 \cos\beta_m - \delta_3 \cos\beta_n - \delta_4 \cos\beta_m) \\ Z &= k_x\,(\delta_1 \sin\beta_n - \delta_2 \sin\beta_m + \delta_3 \sin\beta_n - \delta_4 \sin\beta_m) \end{aligned} \quad (6)$$

For a typical cross-shaped tail rudder, the forces in the y and z directions are

$$\begin{cases} Y = k \times \delta_s \\ Z = k \times \delta_r \end{cases} \quad (7)$$

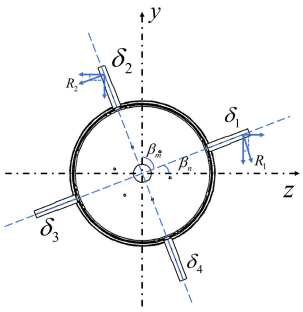

FIGURE 15. The forces on the TDAV tail rudder plane.

If the difference in the flow field between the two arrangements are ignored, $k_x = k$. Then, from (6) and (7) we obtain

$$\begin{aligned} \delta_r &= \delta_1 \sin\beta_n - \delta_2 \sin\beta_m + \delta_3 \sin\beta_n - \delta_4 \sin\beta_m \\ \delta_s &= -\delta_1 \cos\beta_n - \delta_2 \cos\beta_m - \delta_3 \cos\beta_n - \delta_4 \cos\beta_m \end{aligned} \quad (8)$$

For differential motion, the TDAV rudder forces in the Y and Z directions are

$$\begin{aligned} \delta_{d13(z)} &= R_1 \sin\beta_n - R_3 \sin\beta_n \\ \delta_{d13(y)} &= R_1 \cos\beta_n - R_3 \cos\beta_n \\ \delta_{d24(z)} &= -R_2 \sin\beta_m + R_4 \sin\beta_m \\ \delta_{d24(y)} &= -R_2 \cos\beta_m + R_4 \cos\beta_m \end{aligned} \quad (9)$$

and for a typical cruciform rudder are given by

$$\begin{aligned} \delta_{d13(z)} &= k_x \times \delta_d \\ \delta_{d13(y)} &= 0 \\ \delta_{d24(z)} &= 0 \\ \delta_{d24(y)} &= k_x \times \delta_d \end{aligned} \quad (10)$$

Combining (9) and (10) gives

$$\delta_d = \delta_1 \sin\beta_n - \delta_2 \cos\beta_m - \delta_3 \sin\beta_n + \delta_4 \cos\beta_m \quad (11)$$

If $\beta_m = \theta$, then $\beta_n = 90° - \theta$, and substituting (11) in (8) gives

$$\begin{bmatrix} \delta_s \\ \delta_r \\ \delta_d \end{bmatrix} = H \begin{bmatrix} \delta_1 \\ \delta_2 \\ \delta_3 \\ \delta_4 \end{bmatrix} \quad (12)$$

where

$$H = \begin{bmatrix} -\sin\theta & -\cos\theta & -\sin\theta & -\cos\theta \\ \cos\theta & -\sin\theta & \cos\theta & -\sin\theta \\ \cos\theta & -\cos\theta & -\cos\theta & \cos\theta \end{bmatrix} \quad (13)$$

The required rudder angle assignment is then

$$\begin{bmatrix} \delta_1 \\ \delta_2 \\ \delta_3 \\ \delta_4 \end{bmatrix} = T \begin{bmatrix} \delta_s \\ \delta_r \\ \delta_d \end{bmatrix} \quad (14)$$

where

$$T = H^{-1} = \begin{bmatrix} -1/2\sin\theta & 1/2\sin\theta & 1/4\cos\theta \\ -1/2\cos\theta & -1/2\sin\theta & -1/4\cos\theta \\ -1/2\sin\theta & 1/2\cos\theta & -1/4\cos\theta \\ -1/2\cos\theta & -1/2\sin\theta & 1/4\cos\theta \end{bmatrix} \quad (15)$$

However, when the TDAV rolls exactly $\pm 90°$ or $\pm 270°$, i.e. $\theta = \pm 90°$ or $\theta = \pm 270°$, respectively, infinity occurs in the above equation so they are modified which gives

$$\begin{bmatrix} \delta_1 \\ \delta_2 \\ \delta_3 \\ \delta_4 \end{bmatrix} = \begin{bmatrix} -1/2\sin\theta & 1/2\sin\theta & 1/4\cos\theta \\ -1/2\cos\theta & -1/2\sin\theta & -1/4\cos\theta \\ -1/2\sin\theta & 1/2\cos\theta & -1/4\cos\theta \\ -1/2\cos\theta & -1/2\sin\theta & 1/4\cos\theta \end{bmatrix} \times \begin{bmatrix} \delta_s \\ \delta_r \\ \delta_d \end{bmatrix}, \quad \theta \neq \pm 90° \cap \pm 270°$$

$$\times \begin{bmatrix} -1/2\sin\theta & 1/2\sin\theta & 1/4 \\ -1/2\cos\theta & -1/2\sin\theta & -1/4 \\ -1/2\sin\theta & 1/2\cos\theta & -1/4 \\ -1/2\cos\theta & -1/2\sin\theta & 1/4 \end{bmatrix} \times \begin{bmatrix} \delta_s \\ \delta_r \\ \delta_d \end{bmatrix}, \quad \theta = \pm 90° \cap \pm 270° \quad (16)$$

The relationship between the desired TDAV underwater attitude motion $(\delta_s, \delta_r, \delta_d)$ and the actual rotation angles of the rudder blades $(\delta_1, \delta_2, \delta_3, \delta_4)$ can be obtained from (16). The angle θ is the current roll angle of the fuselage relative to the cross-shaped rudder that has been tilted. Once a roll has occurred, the correspondence between the desired direction of motion and the actual rudder blade deflection angle is given by (16). This rudder blade assignment is suitable for the TDAV as will be verified experimentally in the next section.

IV. EXPERIMENTAL RESULTS AND DISCUSSION

In this section, the performance of the TDAV flight control system, attitude switching system, and underwater sailing system are tested separately. Then, the reliability and stability of the combined TDAV system is verified. Fig. 16 presents the TDAV testing steps.

A. FLIGHT CONTROL SYSTEM

Fig. 17 shows several HD camera images of the folding propeller. These test results indicate that when the throttle is more than 20%, the folding propeller opens successfully due to centrifugal motion.

The maximum climbing force is a key operating parameter. Fig. 18 shows that the climbing force and RPM gradually increase as the throttle increases. When the throttle reaches 100%, the force and RPM reach their maximum values which satisfy the design requirements. Fig. 19 presents the power for two operating conditions. Fig. 19(a) is the power for a single rotor motor as the throttle increases. The power of the coaxial counter-paddle motor is approximately twice this value. Fig. 19(b) presents the power for the underwater

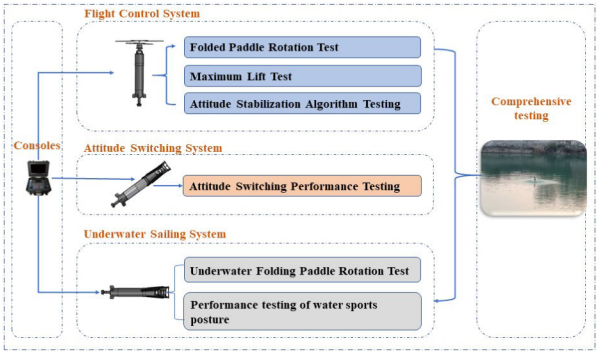

FIGURE 16. The TDAV testing steps.

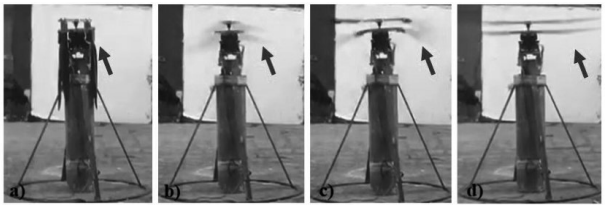

FIGURE 17. Folding blade opening on land with approximate throttle: a) 0%, b) 10%, c) 15%, and d) 20%.

thrusters. This shows that when the throttle is equal to 50%, the thruster stops working and the discharge power is 0. As the throttle increases beyond this point, the thruster rotates forward and the power increases. Similarly, as the throttle decreases, the thruster rotates in the reverse direction and the power increases. Considering that there are significant voltages and current in the system, the modules are designed to have isolated power supplies with all ports connected to the battery via anti-flash high-power connectors.

The TDAV is much heavier than a conventional UAV, so for safety reasons it is important to verify and test the flight control algorithms. Fig. 20 shows that the angular ring output accurately follows the required attitude angle according to the control algorithm even when the angular velocity is large. This confirms the feasibility and effectiveness of the control algorithm.

B. ATTITUDE SWITCHING SYSTEM

The attitude switching system adjusts the TDAV body attitude to achieve the transition from sail to flight or the opposite process. Fig. 21 shows HD camera images of the TDAV transition from sail to flight in water, and the reliability of the attitude adjustment system is proven by the 100% success rate. Fig. 22 presents the time taken to complete this task with a conventional velocity control algorithm which controls the motor at a constant speed and the proposed S-curve control algorithm. This shows that the proposed algorithm is faster and more stable than the conventional algorithm as only 25 s is required to complete TDAV attitude switching.

C. UNDERWATER NAVIGATION SYSTEM

Fig. 23 shows HD camera images of the TDAV propeller opening in water. Although water resistance is a challenge,

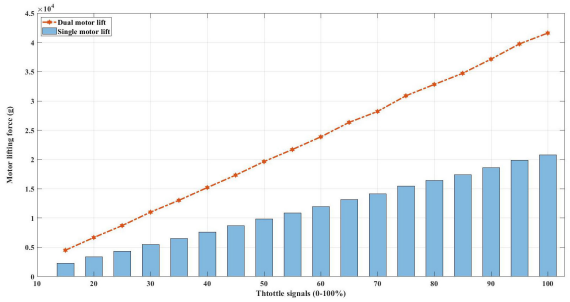

FIGURE 18. The TDAV climbing force.

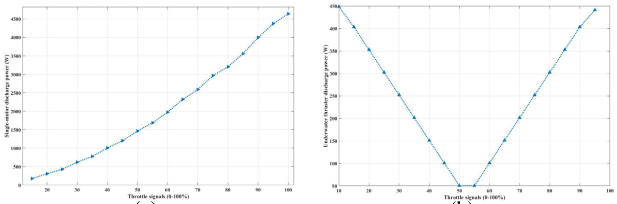

FIGURE 19. The (a) coaxial counter-propeller single motor power, and (b) underwater thruster power.

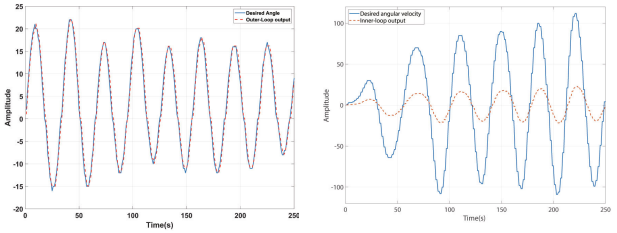

FIGURE 20. Flight attitude adjustment tests: (a) outer loop trajectory tracking, and (b) inner loop trajectory tracking.

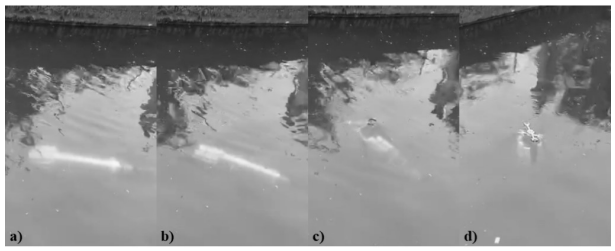

FIGURE 21. The transition from sail to flight.

when the throttle was at 25% the propeller opened smoothly and was able to drive the TDAV body to the water surface which meets the requirements of the trans-domain platform.

In response to the increasing throttle signal, the airframe continuously breaks free from the water resistance to complete the out-of-water movement. In this process, the proposed attitude control algorithm ensures that the TDAV is stable upward which meets the motion requirement of water exit.

D. COMPREHENSIVE TESTING

The comprehensive tests were conducted on November 18, 2019, at Jimo Lake in Qingdao, Shandong, China. It was a sunny day with no wind.

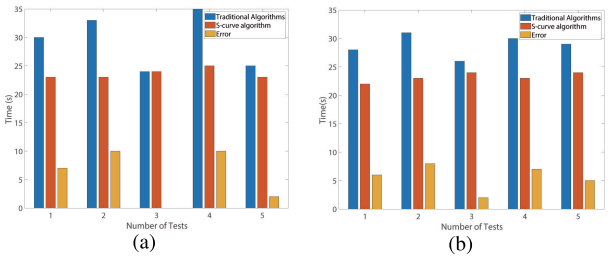

FIGURE 22. Time required for attitude switching for the proposed and conventional algorithms (a) horizontal to vertical, and (b) vertical to horizontal.

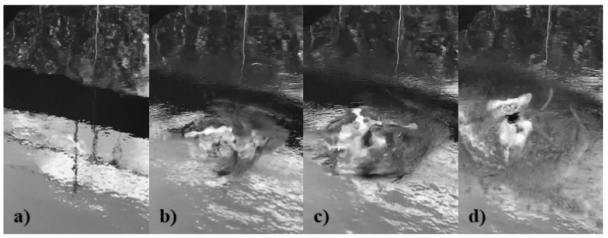

FIGURE 23. TDAV propeller in water with the throttle at approximately a) 0%, b) 15%, c) 20%, and d) 25%.

The TDAV relies on the thrusters and rudder to provide six degrees of freedom movement for the airframe underwater. Fig. 24 shows that the proposed rudder blade assignment algorithm successfully overcomes the TDAV roll phenomenon and achieves appropriate motion in water. The platform sails to a predetermined position and then enters trans-domain mode according to the control command. Then, the attitude switching system adjusts the center of gravity, making the platform vertical by balancing the force and torque. The results of several trans-domain attitude switching tests indicates that the platform can complete trans-domain attitude switching within 25 s, which satisfies the trans-domain movement requirements.

Fig. 25 shows the outdoor flight test. The results indicate that when the throttle is at 30%, the TDAV moves upward, and at 55% it exits the water and hovers at a height greater than 10 m. Thus, trans-domain operation from sail to flight modes was completed successfully. Fig. 26 shows the TDAV landing and recovery. After completing the mission, it slowly descended to the water surface and landed successfully. Thus, trans-domain operation from flight to sail mode was also successful.

Multiple tests were conducted to confirm that the TDAV can takeoff within a short period of time as shown in Table 6. After attitude switching, 5 s was required for the propellers to open, and 25 s for the coaxial counter-propeller motor to reach the speed required to exit the water. Then after 35 s, the TDAV exited the water surface and entered flight mode. Following landing in water, the coaxial counter-propeller motor stopped and the blades folded after 120 s, and 25 s to complete the attitude switch from flight mode to sailing mode. After entering sail mode, underwater motion commenced within 10 s. Overall, the TDAV was able to complete the attitude transition and navigate underwater within 3 min.

FIGURE 24. Lake test for trans-domain motion.

FIGURE 25. TDAV movement exiting the water and hovering.

FIGURE 26. The TDAV landing on water.

TABLE 6. The time required for trans-domain movement tasks.

Task	Definition	Time (s)
Exiting the water	Attitude switching	25
	Paddling in water	5
	Motor achieving the required RPM	20
	Out of the water	10
Entering the water	Motor stopping and blade folding	120
	Attitude switching	25
	Underwater motion	10

The comprehensive test results given in this section verify that the TDAV can successfully achieve trans-domain motion. The platform response times for attitude switching and maneuvering underwater and in the air were excellent, and all design requirements were met.

V. CONCLUSION

In this paper, a novel amphibious UAV prototype was developed which overcomes the difficulties with trans-domain motion such as the suitable performance, water resistance, and effective control. A coaxial counter-propeller-tilting platform was developed based on the trans-domain requirements. Further, an attitude control algorithm was proposed for TDAV flight and trans-domain attitude switching. A rudder distribution algorithm was designed to improve the underwater attitude control performance in the roll state. Both simulation and experimental results were presented which show that the TDAV can easily switch between flight mode, sail mode and trans-domain mode with high stability and reliability. A 433 MHz remote control with range extension was employed for communication with the vehicle, and the underwater control distance was limited to within 2 m. A more reliable and effective way to communicate underwater is one of the future research directions.

APPENDIX A
CFD SIMULATIONS

The airborne performance of the TDAV depends on the relationship between the propeller blades and the coaxial motor. In particular, the propeller size is critical in obtaining the required lift. The aerodynamic performance of the airframe with several commercially available folding propellers was evaluated numerically using the Fluent software package. Based on previous experience and research, the inlet of the flow field can be set as the pressure inlet, and the outlet of the flow field set as the pressure outlet. Considering the Reynolds number criterion, a $k-\epsilon$ RNG model was developed to simulate the flow field under turbulent conditions. Using this approach, it was determined that the TDAV walls are static and the flow field moves at a certain speed. The convergence criterion in the simulations was 0.0001. Fig. 27 shows the gas velocity and pressure nephogram generated by the propeller around the fuselage when the TDAV is hovering in the air at 4000 rpm. Fig. 27(a) indicates that when the propeller rotates, the air above the propeller generates thrust as it flows through the propeller. The airflow is in the direction of the fuselage axis towards the tail and spreads out from the propeller, which lifts the blades. This can also be seen from the pressure nephogram in Fig. 27(b) which shows that the pressure above the blades is smaller and the pressure below is larger, and this pressure difference creates upward lift.

The HobbyWing 30 inch blade was chosen based on the simulation results and the corresponding motor torque ratio is $H/D = 0.08$. This is due to the TDAV length requirements which resulted in the rotors being close together. The aerodynamic performance with this blade is given in Table 7. This shows that the lift force of the upper propeller is greater than that of the lower propeller, but the torque required for the upper propeller is smaller than that of the lower propeller. Thus, the aerodynamic efficiency of the lower propeller is lower. This is because the lower propeller must operate in the turbulent flow generated by the upper propeller. The control algorithm was designed to compensate for the corresponding instability.

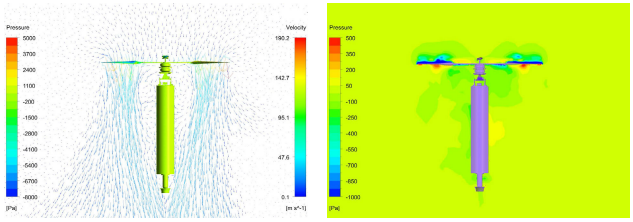

(a) (b)

FIGURE 27. The (a) velocity and (b) pressure nephogram around the TDAV fuselage in air.

When the TDAV is underwater, the flight lift propellers are folded around the fuselage to reduce the drag. Similar to the air flight simulation, the inlet of the flow field was set as the velocity inlet, the outlet of the flow field was set as the pressure outlet, and the convergence criterion is 0.0001. The velocity of the incoming flow was set to 1.57 m/s and the speed of the underwater thruster was set to 3900 RPM. Fig. 28 shows the water velocity and pressure nephogram around the TDAV fuselage. Fig. 28(a) indicates that the incoming flow strikes the rotor disc and decelerates in front of it while Fig. 28(b) shows that the pressure in front of the disc is increasing which creates flow resistance. Thus, the incoming flow striking the rotor disc is the main source of resistance when the platform maneuvers underwater.

TABLE 7. The aerodynamic performance of the propeller.

Parameter	Value	Parameter	Value
Upper blade pull	101.3 N	Lower blade pull	97.6 N
Upper blade torque	14.3 N·m	Lower blade torque	18 N·m
Upper blade power	4.49 kW	Lower blade power	5.65 kW

Numerical simulation was used to design the rotor disc. Based on the goal of reducing flow resistance, a flat stretched rotor disc was chosen rather than a circular rotor disc as in other airframes. Further, a length of 23 cm was determined to provide the least flow resistance. The simulation results are an excellent basis for designing the TDAV body.

APPENDIX B
SEEKER OPTIMIZATION ALGORITHM

The PSO algorithms have been shown to provide excellent performance in numerous applications [46], [47]. A PSO algorithm is initialized with a group of random particles (random solution) and an optimal solution is found iteratively. To achieve this, the particle velocities and positions ar updated using

$$\begin{aligned} v_{id} &= w \times v_{id} + c_1 r_1 \left(p_{id} - x_{id}\right) + c_2 r_2 \left(p_{gd} - x_{id}\right) \\ x_{id} &= x_{id} + v_{id} \end{aligned} \tag{17}$$

where r_1, r_2 are random values in the range (0, 1), w is the inertia weight, and c_1, c_2 are the learning factors. The weight w balances global and local search, with a smaller w biased towards local search and a larger value biased towards global search. In this paper, a PSO algorithm is used to obtain the

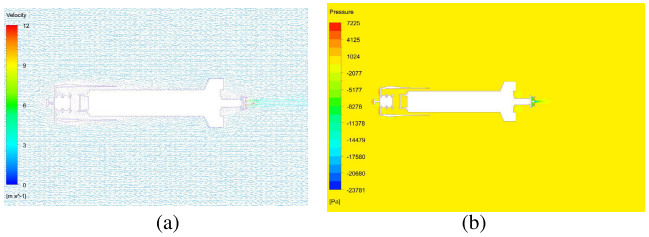

(a) (b)

FIGURE 28. The (a) velocity and (b) pressure nephogram around the TDAV fuselage in water.

Algorithm 1 Improved PSO Algorithm for Tuning FOPID Parameters

1: Set parameters: c_1, c_2, w, *SwarmSize*, *Dim*, $iter_{\max}$
2: Randomly initialize particle positions and velocities: x, v
3: Initialize 7 matrices with zeroes: k_p1, k_i1, λ_2, μ_2, k_p2,k_i2, k_d2
4: While $iter < iter_{\max}$ do
5: Update v_{id}, x_{id} using (4)
6: Update w using (5)
7: If x_{id} exceeds a boundary then
8: Assign the boundary value to x_{id}
9: End if
10: Use the position of the particle as the new PID controller parameters:
$x_{id} \rightarrow [kp_1, k\ i_1, \lambda_2, \mu_2, k\ p_2, k\ i_2, k\ d_2]$
11: Simulate the TDAV with the new controller parameters
12: Evaluate the fitness function from the UAV simulation:
$J = \int_0^\infty t\ (t\ |e_1(t)| + |e_2(t)|)\ dt$
13: Update the individual particles: p_{best}
14: Update the particle population: g_{best}
15: $iter = iter + 1$
16: End While
17: Select g_{best} as the control parameters.

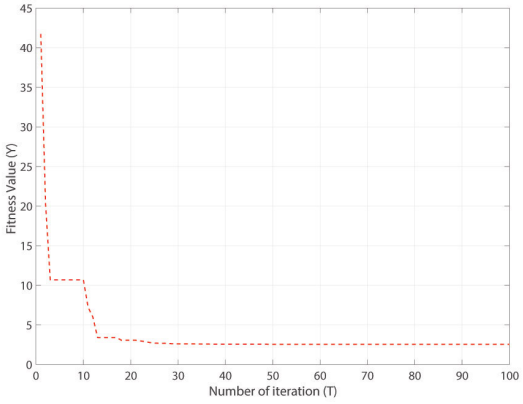

FIGURE 29. Fitness versus the number of iterations with the proposed optimization algorithm.

hierarchical FOPID parameters of the attitude control loop (See Appendix B). The learning factors are set to $c_1 = c_2 = 1.414$. Since dynamic weights can provide better results than fixed weights, the weights are obtained from

$$w = w_{\max} - \frac{iter \times (w_{\max} - w_{\min})}{iter_{\max}} \tag{18}$$

where $iter$ is the current iteration number, $iter_{\max}$ is the maximum number of iterations, $w_{\max}$ is the maximum value of the inertia weight, and $w_{\min}$ is the minimum value of the inertia weight. In order to further accelerate convergence of the search process, an improved fitness function J is employed in the optimization algorithm. Pseudo-code for the proposed PSO algorithm to optimize the hierarchical FOPID parameters is given in Algorithm 1. A Simulink simulation model was built to validate the TDAV model and the reliability of the control algorithm. The fitness versus the number of iterations for this model is shown in Fig. 29 for particle dimension $Dim = 7$, particle swarm size $SwarmSize = 300$ and $iter_{\max} = 300$. This shows that it takes approximately 30 iterations to converge.

REFERENCES

[1] C. Chant, *The World's Greatest Aircraft*. London, U.K.: Caxton Editions, 1999.

[2] P. K. R. Maddikunta, S. Hakak, M. Alazab, S. Bhattacharya, T. R. Gadekallu, W. Z. Khan, and Q.-V. Pham, "Unmanned aerial vehicles in smart agriculture: Applications, requirements, and challenges," *IEEE Sensors J.*, vol. 21, no. 16, pp. 17608–17619, Aug. 2021.

[3] E. J. Provost, P. A. Butcher, M. A. Coleman, D. Bloom, and B. P. Kelaher, "Aerial drone technology can assist compliance of trap fisheries," *Fisheries Manage. Ecology*, vol. 27, no. 4, pp. 381–388, Aug. 2020.

[4] B. Wang, Y. Sun, N. Zhao, and G. Gui, "Learn to coloring: Fast response to perturbation in UAV-assisted disaster relief networks," *IEEE Trans. Veh. Technol.*, vol. 69, no. 3, pp. 3505–3509, Mar. 2020.

[5] Y. Zhao, H. Miu, J. Ma, and H. Du, "Design of the reconnaissance UAV based on TGAM," *J. Phys., Conf. Ser.*, vol. 1771, no. 1, Feb. 2021, Art. no. 012003.

[6] T. Matsuda, T. Maki, Y. Sato, T. Sakamaki, and T. Ura, "Alternating landmark navigation of multiple AUVs for wide seafloor survey: Field experiment and performance verification," *J. Field Robot.*, vol. 35, no. 3, pp. 359–395, May 2018.

[7] V. Vigliotti, "Demonstration of submarine control of an unmanned aerial vehicle," *IEEE Trans. Ind. Electron.*, vol. 19, no. 4, pp. 501–512, Oct. 1998.

[8] H. Liu, "Investigation on the mechanism of a bionic trans-media vehicle and prototype project," *IEEE Trans. Ind. Electron.*, 2009.

[9] G. Yao, J. Liang, T. Wang, X. Yang, M. Liu, and Y. Zhang, "Submersible unmanned flying boat: Design and experiment," in *Proc. IEEE Int. Conf. Robot. Biomimetics (ROBIO)*, Dec. 2014, pp. 1308–1313.

[10] A. Gao and A. H. Techet, "Design considerations for a robotic flying fish," in *Proc. OCEANS MTS/IEEE KONA*, Sep. 2011, pp. 1–8.

[11] T. A. Weisshaar, "Morphing aircraft systems: Historical perspectives and future challenges," *J. Aircr.*, vol. 50, no. 2, pp. 337–353, Mar. 2013.

[12] X. Yang, T. Wang, J. Liang, G. Yao, and W. Zhao, "Submersible unmanned aerial vehicle concept design study," in *Proc. Aviation Technol., Integr., Oper. Conf.*, 2013, p. 4422.

[13] ADMIN. (2014). *Aquacopter Unveils New Waterproof Aerial Drone With Significantly Increased Capabilities and Options*., Accessed: Oct. 3, 2014. [Online]. Available: http://www.ijsba.com/2014/10/03/aquacopter-unveils-new-waterproof-aerial-dro%ne-with-significantly-increased-capabilities-and-options.html

[14] ADMIN. (2015). *Quadh2o Multirotors*. Accessed: Feb. 24, 2015. [Online]. Available: http://www.quadh2o. com/category/resources.html

[15] ADMIN. (2014). *Waterproof Mariner Quadcopter*. Accessed: Nov. 23, 2014. [Online]. Available: http://www.best-quadcopter-reviews.org/waterproof.html

[16] Z. Ma, J. Feng, and J. Yang, "Research on vertical air–water trans-media control of hybrid unmanned aerial underwater vehicles based on adaptive sliding mode dynamical surface control," *Int. J. Adv. Robotic Syst.*, vol. 15, no. 2, 2018, Art. no. 1729881418770531.

[17] P. L. J. Drews, A. A. Neto, and M. F. M. Campos, "Hybrid unmanned aerial underwater vehicle: Modeling and simulation," in *Proc. IEEE/RSJ Int. Conf. Intell. Robots Syst.*, Sep. 2014, pp. 4637–4642.

[18] M. Gilad, L. Shani, A. Schneller, I. Teller, E. Sinai, R. Hachmon, A. Elimelech, O. Rand, C. Friedman, P. Branson, and M. Mistry, "Waterspout-advanced deployable compact rotorcraft in support of special operation forces," in *Proc. 48th Isr. Annu. Conf. Aerosp. Sci.*, Dec. 2008, pp. 1566–1589.

[19] J. Li, Q. Yang, B. Fan, and Y. Sun, "Robust state/output-feedback control of coaxial-rotor MAVs based on adaptive NN approach," *IEEE Trans. Neural Netw. Learn. Syst.*, vol. 30, no. 12, pp. 3547–3557, Dec. 2019.

[20] K. Li, Y. Wei, C. Wang, and H. Deng, "Longitudinal attitude control decoupling algorithm based on the fuzzy sliding mode of a coaxial-rotor UAV," *Electronics*, vol. 8, no. 1, p. 107, Jan. 2019.

[21] Y. Wei, H. Chen, K. Li, H. Deng, and D. Li, "Research on the control algorithm of coaxial rotor aircraft based on sliding mode and PID," *Electronics*, vol. 8, no. 12, p. 1428, Nov. 2019.

[22] M. R. Mokhtari and B. Cherki, "Sliding mode control for a small coaxial rotorcraft UAV," in *Proc. 3rd Int. Conf. Control, Eng. Inf. Technol. (CEIT)*, May 2015, pp. 1–6.

[23] A. Koehl, H. Rafaralahy, M. Boutayeb, and B. Martinez, "Aerodynamic modelling and experimental identification of a coaxial-rotor UAV," *J. Intell. Robotic Syst.*, vol. 68, no. 1, pp. 53–68, 2012.

[24] P. Gnemmi, K. Meder, and C. Rey, "Aerodynamic performance of a gun launched micro air vehicle," *Int. J. Micro Air Vehicles*, vol. 4, no. 4, pp. 251–272, Dec. 2012.

[25] A. Koehl, M. Boutayeb, H. Rafaralahy, and B. Martinez, "Wind-disturbance and aerodynamic parameter estimation of an experimental launched micro air vehicle using an EKF-like observer," in *Proc. 49th IEEE Conf. Decis. Control (CDC)*, Dec. 2010, pp. 6383–6388.

[26] A. Drouot, E. Richard, and M. Boutayeb, "An approximate backstepping based trajectory tracking control of a Gun Launched micro aerial vehicle in crosswind," *J. Intell. Robot. Syst.*, vol. 70, nos. 1–4, pp. 133–150, 2013.

[27] P. Gnemmi, S. Changey, K. Meder, E. Roussel, C. Rey, C. Steinbach, and C. Berner, "Conception and manufacturing of a projectile-drone hybrid system," *IEEE/ASME Trans. Mechatronics*, vol. 22, no. 2, pp. 940–951, Apr. 2017.

[28] A. Drouot, E. Richard, and M. Boutayeb, "Hierarchical backstepping-based control of a Gun Launched MAV in crosswinds: Theory and experiment," *Control Eng. Pract.*, vol. 25, pp. 16–25, Apr. 2014.

[29] P. Gnemmi, A. Koehl, B. Martinez, S. Changey, and S. Theodoulis, "Modeling and control of two GLMAV hover-flight concepts," in *Proc. Eur. Micro Aerial Vehicle Conf.*, 2009, pp. 1–8.

[30] A. Drouot, E. Richard, and M. Boutayeb, "Nonlinear backstepping based trajectory tracking control of a gun launched micro aerial vehicle," in *Proc. AIAA Guid., Navigat., Control Conf.*, Aug. 2012, p. 4455.

[31] A. Bouman, P. Nadan, M. Anderson, D. Pastor, J. Izraelevitz, J. Burdick, and B. Kennedy, "Design and autonomous stabilization of a ballistically-launched multirotor," in *Proc. IEEE Int. Conf. Robot. Autom. (ICRA)*, May 2020, pp. 8511–8517.

[32] D. Pastor, J. Izraelevitz, P. Nadan, A. Bouman, J. Burdick, and B. Kennedy, "Design of a ballistically-launched foldable multirotor," in *Proc. IEEE/RSJ Int. Conf. Intell. Robots Syst. (IROS)*, Nov. 2019, pp. 5212–5218.

[33] G. Cai, A. K. Cai, B. M. Chen, and T. H. Lee, "Construction, modeling and control of a mini autonomous UAV helicopter," in *Proc. IEEE Int. Conf. Autom. Logistics*, Sep. 2008, pp. 449–454.

[34] N. C. Joel, H. Djalo, and K. J. Aurelien, "Robust control of UAV coaxial rotor by using exact feedback linearization and PI-observer," *Int. J. Dyn. Control*, vol. 7, no. 1, pp. 201–208, Mar. 2019.

[35] Z. Song and K. Sun, "Adaptive fault tolerant control for a small coaxial rotor unmanned aerial vehicles with partial loss of actuator effectiveness," *Aerosp. Sci. Technol.*, vol. 88, pp. 362–379, May 2019.

[36] I. Podlubny, "Fractional-order systems and fractional-order controllers," *Inst. Experim. Phys., Slovak Acad. Sci., Kosice*, vol. 12, no. 3, pp. 1–18, 1994.

[37] C. A. Monje, Y. Chen, B. M. Vinagre, D. Xue, and V. Feliu-Batlle, *Fractional-Order Systems and Controls: Fundamentals and Applications*. Springer, 2010.

[38] F. Meng, S. Liu, A. Pang, and K. Liu, "Fractional order PID parameter tuning for solar collector system based on frequency domain analysis," *IEEE Access*, vol. 8, pp. 148980–148988, 2020.

[39] X. Wu, Y. Xu, J. Liu, C. Lv, J. Zhou, and Q. Zhang, "Characteristics analysis and fuzzy fractional-order PID parameter optimization for primary frequency modulation of a pumped storage unit based on a multi-objective gravitational search algorithm," *Energies*, vol. 13, no. 1, p. 137, Dec. 2019.

[40] K.-H. Rew and K.-S. Kim, "Using asymmetric S-curve profile for fast and vibrationless motion," in *Proc. Int. Conf. Control, Autom. Syst.*, Oct. 2007, pp. 500–504.
[41] W. Bangji, L. Qingxiang, Z. Lei, Z. Yanrong, L. Xiangqiang, and Z. Jianqiong, "Velocity profile algorithm realization on FPGA for stepper motor controller," in *Proc. 2nd Int. Conf. Artif. Intell., Manage. Sci. Electron. Commerce (AIMSEC)*, Aug. 2011, pp. 6072–6075.
[42] T.-C. Chen and Y.-C. Su, "High performance algorithm realization on FPGA for stepper motor controller," in *Proc. SICE Annu. Conf.*, Aug. 2008, pp. 1390–1395.
[43] Z. Tao and L. Junxing, "Study on the equivalent rudder angle between X type and cruciform rudders on submarine," *IEEE Trans. Ind. Electron.*, vol. 5, 2004.
[44] Y. Zhang, Y. Li, Y. Sun, J. Zeng, and L. Wan, *Design and Simulation of X-Rudder AUV's Motion Control*, vol. 137. Amsterdam, The Netherlands: Elsevier, 2017, pp. 204–214.
[45] Y. Zhang, Y. Li, G. Zhang, J. Zeng, and L. Wan, *Design of X-Rudder Autonomous Underwater Vehicle's Quadruple-Rudder Allocation With Lévy Flight Character*, vol. 14, no. 6. London, U.K.: SAGE, 2017, Art. no. 1729881417741738.
[46] D. Tian and Z. Shi, "MPSO: Modified particle swarm optimization and its applications," *Swarm Evol. Comput.*, vol. 41, pp. 49–68, Aug. 2018.
[47] B. Salamat and A. M. Tonello, "Adaptive nonlinear PID control for a quadrotor UAV using particle swarm optimization," in *Proc. IEEE Aerosp. Conf.*, Mar. 2019, pp. 1–12.

YONG GAO was born in Ulanqab, Inner Mongolia Autonomous Region, China, in 1991. He received the B.S. degree from Inner Mongolia University, in 2014, and the M.S. degree from the Ocean University of China, Qingdao, China, in 2018, where he is currently pursuing the Ph.D. degree with the School of Information Science and Engineering. He has applied for one national invention patent. His research interests include design of flying vehicles, motion control, and optimization algorithms.

HAO ZHANG (Senior Member, IEEE) was born in Jiangsu, China, in 1975. He received the B.S. degree in telecom engineering and industrial management from Shanghai Jiao Tong University, China, in 1994, the M.B.A. degree from the New York Institute of Technology, New York, NY, USA, in 2001, and the Ph.D. degree in electrical engineering from the University of Victoria, Victoria, BC, Canada, in 2004. From 1994 to 1997, he was an Assistant President of ICO (China) Global Communications Company. He is currently a Professor with the Department of Electrical Engineering, Ocean University of China. He is also an Adjunct Professor with the Department of Electrical and Computer Engineering, University of Victoria. His research interests include ultra-wideband systems, MIMO wireless systems, and spread spectrum communications.

HUA YANG received the M.S. degree from Shandong University and the Ph.D. degree from Shanghai Jiao Tong University, Shanghai, China. She is currently an Associate Professor with the Information Science and Engineering College, Ocean University of China, Qingdao, China. She also serves as the Principal Investigator for the National Nature Science Foundation of China. Her research interests include wireless signals modeling and recognition and the development of electronic products and systems.

SHIZHE TAN was born in Shandong, China, in 1971. He received the B.S. and M.S. degrees in mechanical and electrical engineering from Shandong University, Shandong, in 1993 and 1996, respectively, and the Ph.D. degree in mechanical engineering from Shanghai Jiao Tong University, Shanghai, in 2002. From 2002 to 2005, he was engaged in postdoctoral research at the Robot Laboratory, Harbin Institute of Technology. Since 2005, he has been an Assistant Professor with the Electronic Engineering Department, Ocean University of China. He is the author of several books, more than 20 articles, and holds five invention patents. His research interests include underwater sensors and applications. His awards and honors include the First Prize of Science and Technology Progress Award of China Navigation and positioning Association.

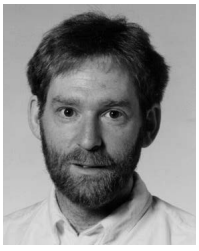

T. AARON GULLIVER (Senior Member, IEEE) received the B.S. and M.Sc. degrees in electrical engineering from the University of New Brunswick, Fredericton, NB, Canada, in 1982 and 1984, respectively, and the Ph.D. degree in electrical and computer engineering from the University of Victoria, Victoria, BC, Canada, in 1989. From 1989 to 1991, he was employed as a Defence Scientist at the Defence Research Establishment Ottawa, Ottawa, ON, Canada. He has held academic positions at Carleton University, Ottawa, and the University of Canterbury, Christchurch, New Zealand. He joined the University of Victoria, in 1999, where he is currently a Professor with the Department of Electrical and Computer Engineering. His research interests include information theory and communication theory, algebraic coding theory, cryptography and security, and smart grid and ultra wideband communications. In 2002, he became a fellow of the Engineering Institute of Canada and the Canadian Academy of Engineering, in 2012.

TINGTING LU was born in 1983. She received the B.S. degree in communication engineering from Hunan University, in 2006, and the M.S. degree in communication and information systems and the Ph.D. degree in computer application technology from the Ocean University of China, in 2009 and 2013, respectively. She is a currently a Lecturer with the Ocean University of China. Her research interests include mmWave communication systems, MIMO wireless systems, OFDM technologies, and GNSS.